Journal of Engineering and Sustainable Development
https://jeasd.uomustansiriyah.edu.iq/index.php/jeasd
https://doi.org/10.31272/jeasd.27.2.9

Vol. 27, No. 02, March 2023
ISSN 2520-0917

Technical Research

EFFECTS OF MULTIPATH PROPAGATION CHANNEL IN TIGRIS RIVER

Murad Shahadha Mahmood[1] ***Yasin Yousif Al-Aboosi**[1,2]

1) Electrical Engineering, Department, College of Engineering, Mustansiriyah University, Baghdad, Iraq
2) Faculty of Electrical Engineering, Universiti Technology Malaysia UTM, Malaysia

Received 14/1/2021 ***Accepted in revised form 25/3/2021*** ***Published 1/3/2023***

Abstract: Tigris River is an environment of shallow waters because of its low depth and it has been identified as a multi-path channel. The underwater multi-path propagation leads to reverberation as well as fading, which causes large transmission loss. The present paper conducts 3 underwater acoustic simulation outcomes in the district of Abu Dali - Kazem Al Ali village - Tigris beaches - Baghdad - Iraq. The distance from the sender to the receiver are (100m, 1000 m, and 5000m). With the use Ray model, results have shown that the multi-path propagations dominate in a case where the distance from sender to receiver, has been increased, which resulted in decreasing the grazing angle, thereby, increasing the coefficient of reflection. The consecutive path amplitude values will not be decreased quickly. This is why differences in the time between different paths are minimal. This indicates that the consecutive path-ways will be converged with time, which will result in an inter-symbol interference phenomenon, playing a role in an increase of the received data bit error rate.

Keywords: *Multipath propagation; propagation delay; acoustic path loss; reflection, grazing angle.*

1. Introduction

An underwater acoustic communication system (UWACS) was initially widely applied by the army in the late 19th century. The earliest use of the UWACS was intended solely for naval and nautical personnel. Traditional UWA applications included installing underwater bells on the lightship. Sounds that are made by those bells throughout the navigation have then been detected over some considerable distance by a stethoscope or by a simple microphone that is mounted on the ship's hull. This method was able to help avoid navigational hazards in low visibility conditions. Sound propagates by molecular transfer of emotional energy. Sound requires a medium for propagation because it can't be passing through the vacuum. Acoustically, the media by which the sound travels include solids, liquids, plasma, and gases [1-3]. For underwater media, acoustic waves are more convenient for some applications such as communications, navigation, and other wireless applications as a result of the high rate of attenuation of the electromagnetic waves. Acoustic propagations are affected by several factors, the most important of which are attenuation, multi-path propagations, and a low sound speed is approximately 1500m/s. the attenuation has been found proportionate to the frequency of the signal while multipath propagation is changed over time [4]. In the

**Corresponding Author*: ymyasin2@live.utm.my

underwater medium, the fading is dependent upon the frequency, range of the communication, and location of the sensor. It may be split into two types, the first type is Short- term fading, which consists of Doppler spread and multipath propagation that is changed over distance and time, and the second type is Long-term fading due to sound propagation has been affected by absorption loss and spreading loss, depending upon frequency and range [5].

Fig1. Shows that the acoustic energy may be dispersed and then reflected from the surface of the sea as well as the floor of the sea, which means permitting the likelihood of having more than one transmission channel for one signal [6]. The underwater multi-path propagation results in reverberation as well as fading, which leads to a large transmission loss [8]. In the digital communication, the consecutive interfering pulses result in one of the phenomena of the inter symbol interference (ISI), and that leads to the increase in bit error rate (BER) of data that had been received [9-11]. Which is why, the UWAC typically support low levels of the data [5,12]. The purpose of this research is studying effects of multipath Propagation Channel in Tigris River.

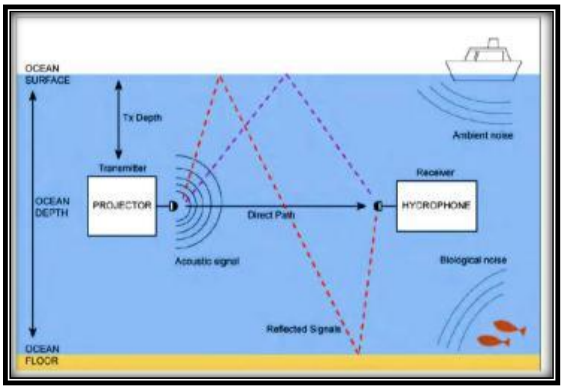

Figure 1. Signal Attenuation Loss on the Propagation of the Acoustic Waves [7].

2. Sound Velocity

Knowledge of wave propagation is essential for clearer understanding of the underwater propagation of sound and for developing an accurate channel model. Typically, underwater sound speed ranges from 1440 to 1550 (m/sec) [13]. In general, changes in the speed of sound are smaller, but small changes in the speed of the sound minimize the strong system. The speed of the sound underwater depends primarily on 3 major parameters temperature, depth, and salinity. Underwater sound velocity is computed according to the following empirical formula [14,15].

$$C = 4.6T - 0.055.T2 + 0.00029.T3 + (1.340 - 0.01.T).(S - 35) + 0.016Z + 1449.20 \quad (1)$$

Here: -

C represents sound speed in seawater (m/sec), S represents water salinity in Part per Thousand (ppt), T represents temperature of water (^{o}C), and Z represents depth (m). For deep water, salinity is generally considered constant at 35 ppt because in deep water, the effect of the salinity on the velocity of sound is insignificant. Equation (1) has validity for:

$$(0 \leq T \leq 35)°C, (0 \leq S \leq 45) ppt \; and$$

$$(0 \leq D \leq 1000)\, m$$

3. Signal Attenuation

Underwater physical and chemical characteristics and Acoustic geometry of channel impact propagation of sound, at wide scale in underwater environment. The acoustic signal is affected by attenuation caused by spreading and absorption [4,16]. Consequently, attenuation is directly relative to frequency that is used by system and the distance of the communication (i.e., the Range) [4, 16, 17, 18].

The absorption loss is caused by the expansion of the region, which the signal of the sound includes when it extends in a geometrical manner outward

from source [19]. The loss of the absorption can be stated in dB by:

$$P_{\text{L spread}} = k \times 10log\,(R) \quad (2)$$

Here: -

R represents range of communication (m) and k represents spread factor, k denotes propagation geometry for acoustic signals. Usually applied to spread factor values are k = 1 for the cylindrical spreading, k = 2 for the spherical spreading and k = 1.50 in the practical spreading [20, 21]. Loss of spread represents logarithmic correlation with the range of communication and it is effects on signal are most noticeable in the short term [4].

The absorption loss ($P_{L\text{-absorb}}$) represents energy loss as the heat from viscous friction and ionic relaxation that occurs in the case where wave that has been generated by acoustic signal is propagated outwards. Those losses are varied in a linear manner with the range $P_{L\text{absorb}}$ can be represented in dB [4,21]:

$$P_{\text{L absorb}} = R \times 10log\alpha\,(f) \quad (3)$$

Where: -

R represents range (km) and α (f) represents the coefficient of absorption [4] and [20,22].

The summation of the spread loss and the absorption loss denoted acoustic path loss values that could be expressed by dB [4, 20,22]:

$$P_{\text{L}} = k \times 10log\,(R) + R \times 10log\alpha\,(f) \quad (4)$$

Experimental formulas of the factor of the attenuation in the seawater have been obtained, based upon the large-scale field experimentations and lab. The formula demonstrates that α (f) is directly related to operating frequency. Which is why, the increase in the frequency leads to the increase in the amount of the absorption [7, 23].

Simmons & Fisher had suggested empirical formula for α (f) (dB/km) which differs with the variations of the pressure, frequency, and temperature. For the frequency values that range between 10kHz and 1MHz [5, 24, 25].

$$\alpha(f) = \frac{x_1 P_1 F_1 F^2}{F_1^2+F^2} + \frac{x_2 P_2 F_2 F^2}{F_2^2+F^2} + x_3 P_3 F^2 \quad (5)$$

Saltwater is a combination of B(OH)3, MgSO4 and H2O [7]. The first formulation term indicates Boric Acid attenuation, while second one indicates Magnesium Sulphate attenuation and the third indicates Pure Water attenuation.

In a case where **$(B(OH)_3)$**

$x_1 = \frac{8.6860}{c} \times 10^{\,0{\cdot}78PH-5}$, $p_1 = 1$ and

$f_{1=\,2.80\,*} \sqrt{\frac{S}{35}} \times 10^{(4-\,1245\,/(T+273))}$

In the case of **$(MgSO_4)$**

$$x_2 = \frac{S}{c}(1 + 0.025T)$$

$P_2 = 1 - 1.37x10^{-4} Z_{max} + 6.2x\,10^{-9} Z^2_{max}$ and

$$f2 = \frac{8{\cdot}17\times10^{\,9-\frac{1193}{(T+237)}}}{1+0{\cdot}0018\,(S-35)}$$

In the case of **(H2O)**

$$P_3 = 1 - 3.83 \times 10^{-5} Z_{max} + 4.9 \times 10^{-10} Z^2_{max}$$

$$x_3 = 4 \cdot 937 \times 10^{-4} - 2.59 \times 10^{-5}\,T + 9.11x10^{-7}T^2 - 1.50 \times 10^{-8}\,T^3 \;if\; T \leq 20° \;or$$

$$x_3 = 3 \cdot 964 \times 10^{-4} - 1.146 \times 10^{-5}T + 1.45 \times 10^{-7}T^2 - 6.5 \times 10^{-8}T^3 \;if\; T \geq 20° \quad (6)$$

Where the coefficient values X_1, X_2 and X_3 represent impacts of the temperature, whereas the

coefficients P_1, P_2 and P_3 represent oceanic depths (i.e., pressure values) and f_1, f_2 represent frequencies of relaxation of the molecules of the boric acid and ($MgSO_4$). Where T (°C), f (kHz), S (ppt), Z_{max}, c and pH represent depth (m), the sound velocity (m/s.) and PH value [5, 23]. Fisher and Simmons model has different kinds of the restriction. For instance, the depth cannot exceed 8 km, and salinity is limited to 35 ppt, the pH value is limited to a fixed value of 8 [16].

4. Sound Attenuation in Sediment

Attenuation of sound in the sediment varies fundamentally according to type of bottom. Type of bottom, denoted by bt, determines sedimentary materials in the ocean. Table1. shows value's type of bottom for every one of the sediment types [23].

Table1. The value's type of bottom for every one of the sediment types.

Bottom Type	Value of bottom type
Very coarse sand	0
Coarse sand	1
Medium sand	2
Fine sand	3
Very fine sand	4
Very coarse silt	5
Coarse silt	6
Medium silt	7
Fine silt	8
Very fine silt	9
Clay	10

5. Ray Model

Multi-path propagation geometry has been considered as significant for the communication systems which utilize the array processing for the purpose of suppressing the multi-path. In the ocean, acoustic propagation is controlled by the wave equation. Generally, it is difficult to find solutions to the wave equation [26]. Ray model approximates multipath propagation in the underwater environment [27]. With a multipath effect, approximations are usually used for modeling the propagation of acoustic signals [13,28].

Fig 2. Displays a diagram representing contribution of physical source in the depth Z_s and first 3 sources of the images.

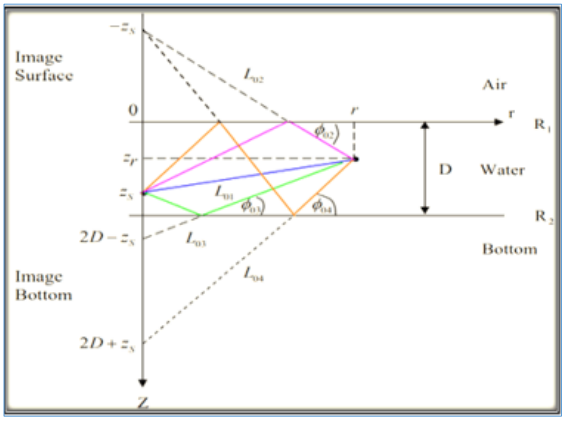

Figure 2. wave reflections from layer bounds and sources of image.

Here, Z_s denotes source depth, D denotes water column height in m, Z_r denotes receiver depth, and r denotes range of transmission. Z_s, D, Z_r, and r measured in meters [29]. Successive imaging of these sources to obtain expansion of the whole field ray [23,30].

$$p_{(r,z,w)} = A(\omega) \sum_{m=0}^{\infty} \{ \hat{R}_1^m (\phi_{m1}, w) \hat{R}_2^m (\phi_{m1}, w)$$

$$\frac{e^{-jkLm1}}{Lm1} + \hat{R}_1^{m+1} (\phi_{m2}, w)\, \hat{R}_2^m (\phi_{m2}, w) \frac{e^{-jkLm2}}{4\pi Lm2} +$$

$$\hat{R}_1^{m+1} (\phi_{m2}, w)\, \hat{R}_2^m (\phi_{m2}, w) \frac{e^{-jkLm2}}{4\pi Lm2} + \hat{R}_1^m (\phi_{m3}, w)$$

$$\hat{R}_2^{m+1} (\phi_{m3}, w) \frac{e^{-jkLm3}}{Lm3} + \hat{R}_1^{m+1} (\phi_{m4}, w)\, \hat{R}_2^{m+1}$$

$$(\phi_{m4},w)\frac{e^{-jkLm4}}{Lm4}\} \quad (7)$$

Here : -

m = 0 to ∞, A(ω) denotes signal amplitude, $\widehat{R}_1$ represents coefficient of surface reflection, $\widehat{R}_2$ represents coefficient of bottom reflection, k denotes acoustic complex wave number, φ_{m1}, φ_{m2}, φ_{m3} and φ_{m1} denote the grazing angle values of all rays, L_{m1}, L_{m2}, L_{m3} & Lm4 denote Length values of all of the rays.

$$L_{m1}=\sqrt{(r)^2+(2D*m-z_s+z_r)^2}, \quad (8)$$

$$L_{m2}=\sqrt{(r)^2+(2D*m+z_s+z_r)^2}, \quad (9)$$

$$L_{m3}=\sqrt{(r)^2+(2D*(m+1)-z_s-z_r)^2}, \quad (10)$$

$$L_{m4}=\sqrt{(r)^2+(2D*(m+1)+z_s-z_r)^2}. \quad (11)$$

$$\varphi_{m1}=\tan^{-1}\left(\frac{(2D*m)-z_s+z_r)}{r}\right), \quad (12)$$

$$\varphi_{m2}=\tan^{-1}\left(\frac{(2D*m)+z_s+z_r)}{r}\right), \quad (13)$$

$$\varphi_{m3}=\tan^{-1}\left(\frac{(2D*(m+1))-z_s-z_r)}{r}\right), \quad (14)$$

$$\varphi_{m4}=\tan^{-1}\left(\frac{(2D*(m+1))+z_s-z_r)}{r}\right). \quad (15)$$

5.1. Travel Times

Every ray's travel time represents time that is needed for reaching receiver [23,30].

$$T_{m1}=\frac{Lm1}{c}, T_{m2}=\frac{Lm2}{c}, T_{m3}=\frac{Lm3}{c}, T_{m4}=\frac{Lm4}{c} \quad (16)$$

Here, c denotes the velocity of the Sound in (m/s).

5.2. Propagation Delays

Under-water network systems have been found to be highly influenced by the long delays of the propagation that result from slow propagation of the sound in under-water environments [31]. Propagation Delay is caused by differences in the path length values. Suppose τ_{m2} be propagation delay along the path L_{m2}, τ_{m3} be propagation delay along path L_{m3} and τ_{m4} represent delay of propagation along path L_{m4}, therefore, we have:

$$\tau_{m1}=\frac{L_{m1}-L_{o1}}{c}, \tau_{m2}=\frac{L_{m2}-L_{o1}}{c}, \tau_{m3}=\frac{L_{m3}-L_{o1}}{c}, \tau_{m4}=\frac{L_{m4}-L_{o1}}{c}. \quad (17)$$

Where L_{01} represents the direct path length. Delays in the propagation of signal path which is different from line of sight path represent a significant parameter for under-water acoustic communication channels. Because of signal arriving with a bit of a delay to receiver, the inter symbol interference (ISI) occurs that impacts system performance and rate of transmission that decrease as well [32].

5.3. Reflection at Sea Surface

The mismatch of impedance between sea-water and air leads to sea surface being considered as good reflector. In a case where ocean and sea surfaces are still, then reflection is near perfection, but involves phase shift by π radians. This means coefficient of reflection is (−1). If roughness is small in relation to a wave-length, then surface could be processed in the form of random scattered and reflection coefficient could be expressed as [33]:

$$L_{SR}=-e^{-0\cdot5\Gamma^2} \quad (18)$$

Where: -

L_{SR} is the surface reflection coefficients and Γ denotes Rayleigh roughness parameter set had been expressed by:

$$\Gamma=2k\sigma\sin(\theta) \quad (19)$$

Where denotes acoustic wavenumber (2 π/λ), θ denotes incident angle and σ rms surface roughness.

$$\sigma = \sqrt{0{\cdot}3240 * 10^{-5} * V_w{}^5} \quad (20)$$

Where V_w represents velocity of the wind (m/s). In terms of intensity, measured in decibels, the surface losses would:

$$S_L=300(f^2\sigma^2[\sin(\theta)]^2) \quad (21)$$

5.4. Reflection at the Sea Bottom

The mismatch of the impedance from bottom and surface water bottom reflecting part of incident. Assuming that ρ_1 and c_1 represent density and velocity of the sound in sea-water, c_2 and p_2 to velocity of sound and seabed density. Rayleigh's reflection coefficient (L_{BR}) for smooth seabed is dependent upon angle and has been expressed as [34].

$$L(\theta) = \left| \frac{m \cos\theta 1 - \sqrt{n^2 - \sin^2\theta 1}}{m \cos\theta 1 + \sqrt{n^2 - \sin^2\theta 1}} \right| \quad (22)$$

Where: -

$$m = \frac{\rho_2}{\rho_1}, n = \frac{c_1}{c_2} \quad (23)$$

For seabed, σ is associated with the size of the particles (the particle represents sediment material) as:

$$\sigma = \frac{2^{-bt}}{1000} \quad (24)$$

here, bt denotes bottom type.

The Rayleigh model has been utilized in order to model loss from seafloor reflection. It takes into account the velocity of sound and the density in interface between the water and the seabed. Rayleigh's Simplified model considers that scattering phenomenon isn't as significant as into sea surface, meaning that the loss is independent of the frequency. The loss of the seabed is calculated by using [35].

$$B_L = -10 \log(L_{BR}(\theta))^2 \quad (25)$$

5.5. Multipath

In the shallow waters, the propagation of the sound is influenced by the reflections of the surface, whereas in the deep waters, the propagation of the sound is influenced by the bottom reflection that becomes one of the main causes of the delay of communications in under-water acoustic communications' system. The key reason behind acoustic signal being weak is referred to as multi-path impact that becomes a cause of the inter-symbol interferences. In addition, it makes acoustic data transmission mistaken and difficult. Horizontal acoustic channel is more influenced by multi-path impact than vertical acoustic channel [36]. The majority of time in the oceans and deep seas as a result of the variation in the sound refraction speed, a multipath impact case happens on acoustic channel. Propagation delays, number of the paths of propagation, and its strength has been found by acoustic channel's impulse response that is affected by the geometry and reflection of the channel. In addition, sound velocity variations with the depth lead to wave refraction. [37]. As a result, receiver performs the detection of multiple pulses that have various amplitudes, phases and arrival times. [38]. Channel impulse response to the under-water multi-path acoustic channel may be represented by the equation below [39,40]:

$$h(\tau, t) = \sum_p A_p(t)\, \delta\left(\tau - \tau_p(t)\right) \quad (26)$$

Where $A_p(t)$ represents the path amplitude and $\tau_p(t)$represents the path delay, both time dependent. Therefore, every path in acoustic channel plays the role of low-pass filter. Transmission range, frequency, depth, channel geometry and sound velocity profile represent the major factors which lead to the multi-path effects [41].

6. Result and Discussion

River variable measurements have been carried out in Abu Dali district -Kazim Al Ali Village- Tigris - Baghdad- Iraq. Latitude:33.5223301°N; longitude:44.3052168°E) on Nov. 1st 2020. As can be seen from Fig3 and Fig4. The velocity of the wind has been about 8 knots, T has been 34°C, S = 0.4944ppt, 6m deep, pH = 6.90 and bottom type is very fine sand. Based on empirical formula, obtained speed of the sound has been 1,519m/s.

Figure 3. Experiment with the test in Abu Dali district

Figure 4. Field experimentations in Abu Dali district Tigris Beaches-Baghdad-Iraq,1st November 2020.

The water specimens have been obtained directly from Tigris river as can be seen from Fig5. It has been observed that the PH value has been 6.90. It has been measured with the use of pH meter as can be seen from Fig6.

Figure 5. Field experiments have shown the water samples that have been obtained directly from the Tigris.

Figure 6. PH meter showing the water specimen that has been taken from Abu Dali district.

The value of salinity in the Tigris has been 0.4944ppt. This value is in the range 0ppt ≤ S ≤ 45ppt, this salinity value is highly different from salinity values of the ocean and sea due to the geological formation nature of sea and ocean waters, differing from river waters [14, 15]. The sample of the water was measured by the use of the Electrical Conductivity (EC) meter and it has been noticed that EC= 824µS/cm as can be seen from Fig 7. There's a direct correlation between TDS and EC may be represented by:

$$TDS = G.EC \quad (27)$$

Where the value of the TDS is measured in (ppm) or (mg/ℓ), EC is measured in (µS/cm), G represents conversion factor into the TDS in a range between 0.50 and 0.70, generally, 0.70 is recommended with EC > 1,000µS/cm and 0.60 with EC lower than the threshold [42], which is why:

TDS= 0.60 (824) = 494.4ppm = 0.4944ppt.

Then, it was taken the same water sample and repeated the measurement, by using Total Dissolved Solids (TDS). It is found that the value of salinity in Tigris river was 482 ppm (0.482 ppt). As shown in Fig 8.

Water sample measurements have been obtained from river for the calculation of the salinity (S) and PH value has been performed in the Environmental Laboratory, Dept. of Environmental Engineering, Faculty of Engineering, Al- Mustansiriyah Univ.

Figure 7. EC meter showing the water samples in the Abu Dali district.

Figure 8. TDS.

The sample of the soil has been directly obtained from Abu Dali district and it has been discovered that the bottom type is very fine sand, the bottom type value has been 4 based on Table1. The experimentation has been carried out in soil lab, Dept. of Civil Engineering, Engineering Faculty, Al- Mustansiriyah Univ., as can be seen from Fig9.

a) Drying Oven.

b) Set of sieves

c) Sieve Shaker

d) Balance

Figure 9. Tools and Devices that have been utilized for find the bottom type at the Tigris River in Abu Dali district.

Fig 10. Illustrates transmission losses in Tigris River as frequency function at various distances between the transmitter and the receiver (R=1km, 10km, 50km and 100km). It has been observed that the path losses are increased with the increase in the communication frequency and distance and reaches extremely high values for ultrasonic frequencies. Transmission loss depends on acoustic signal attenuation, and it is directly proportionate to path length and range of the transmission [19, 21, 43]. Results have shown transmission loss with some variable frequency

in a constant range of 1km, 10km, 50km and 100km computed according to "(4)".

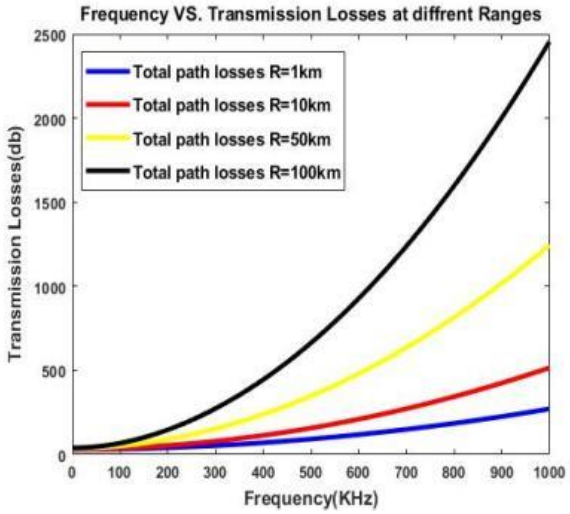

Figure 10. Transmission losses in Tigris as function of frequency at different ranges, PH = 6.9, S= 0.4944ppt, T=34°C and Z= 6m.

Fig11. Indicates losses in Tigris River at variety of the frequencies. It was noted that transmission losses have been increased considerably at high frequency in comparison to low frequency. Consequently, in both sea and ocean, sound attenuation is frequency dependent, sea and ocean act as LPF [4].

Figure 12. Surface Reflection Coefficient at Abu Dali district as Range function at, Z_s=Z_r=5m, D=12m, V_w=8Kn, S= 0.4944ppt, and T=34°C.

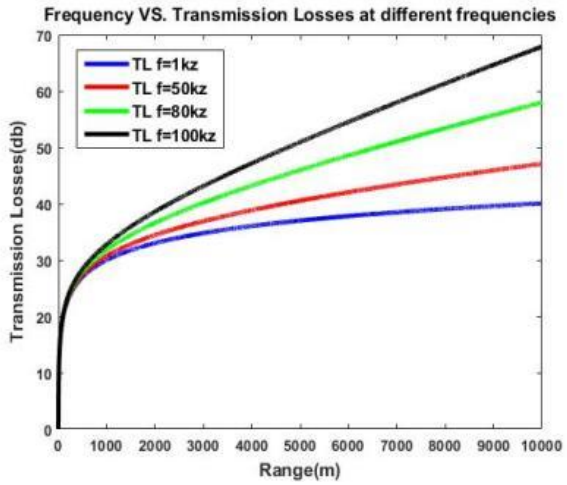

Figure 11. Transmission losses in Tigris River as function of distance at different frequencies, PH = 6.9, S= 0.4944ppt, T=34°C and Z= 6m.

Fig12. Illustrates the coefficient of surface reflection for the direct paths (Dp), bottom reflection path (BRP), surface reflection path (SRP), as well as the surface bottom reflection path (SBRP), at the Abu Dali district in the Tigris, at Z_s = Z_r = 5m and D =12m. It has been noted that the coefficient of surface reflection to (SRP, SBRP and BRP) is increased with the increase of distance from transmitter to receiver. While coefficient of surface reflection of the DP equals 1, due to the fact that the location of the transmitter equals the location of the receiver [23].

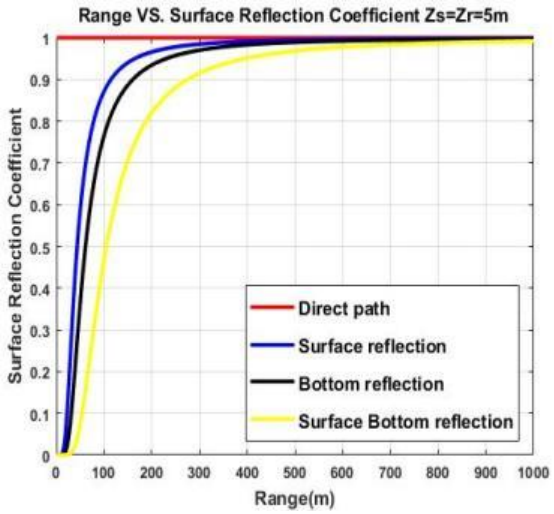

Fig13. Illustrates Grazing Angle versus the Range at the Abu Dali district. In a case where distance from transmitter to receiver increases, grazing angle will be decreased. [23,31].

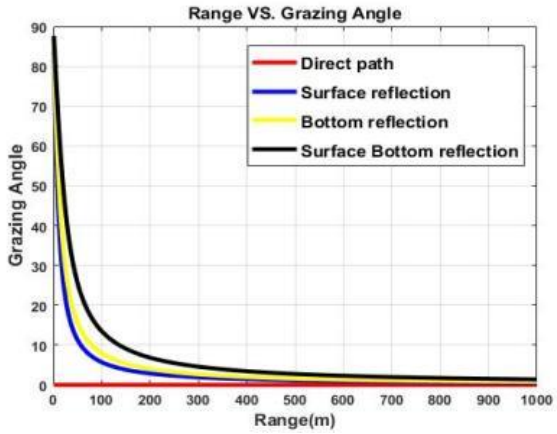

Figure 13. Grazing angle at the Abu Dali district as a Range function at, Z_s=5m, Z_r=5m, D=12m S=0.49440 and T=34ºC.

Fig14. Illustrates coefficient of bottom reflection for the DP, BRP, SRP, and SBRP, at Abu Dali district, at Zs = Zr = 5m and D =12m. It has been noted that the coefficient of bottom reflection is increased with the increase in distance from sender to receiver [23].

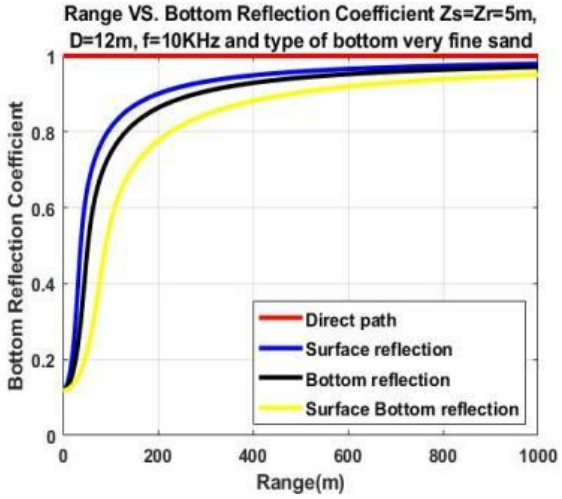

Figure 14. Bottom reflection coefficient at Abu Dali district in the Tigris as a range function at, Z_s=Z_r=5m, D=12m, f=10KHz, bottom type very fine sands, S= 0.4944ppt, and T=34ºC.

Fig15. Shows bottom reflection coefficient versus Grazing angle at Abu Dali district. As distance from transmitter to receiver is increased, grazing angle decreases, thereby increasing the coefficient of reflection [12].

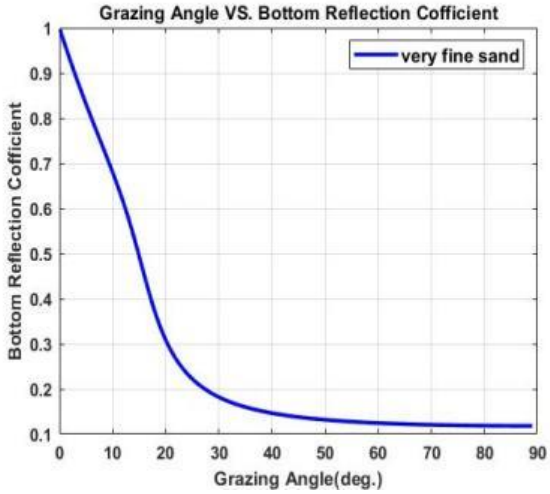

Figure 15. coefficient of Bottom reflection versus the Grazing angle at Abu Dali district at, Z_r=Z_s=5m, D=12m, f=10KHz, bottom type very fine sands, S= 0.4944ppt, and T=34ºC.

Fig 16. Shows the multi-path propagation in Abu Dali district at distance from transmitter to receiver is 100m. Clearly, it has been noted that there has been a process of degradation in the amplitude from the rays 1 until 8. In the case where separation between sender and receiver are (10m-200m), multi-path propagation has little effect, so the complexity of the design of the receiver is greatly decreased [23,30].

The results of simulation show the time delays (T) of all of the eight rays compared with coefficient of surface reflection (R_s), grazing angles (φ), coefficient of bottom reflection (R_b) and the normalized amplitude of the received signal (N.A) are provided in the Table 2.

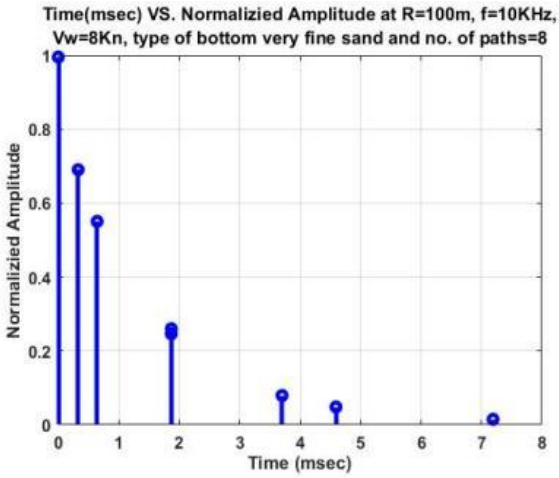

Figure 16. Multi-path propagation in Abu Dali district in Tigris River at, Zr=Zs=5m, D=12m, V_w=8Kn, R=100m, S= 0.4944ppt, T=34ºC, f=10KHz and bottom type is very fine sands.

Clearly, results have proven that reflection coefficient is decreased in the case where the grazing angle increases due to short distance (i.e., 100 m) from sender to receiver [12]. Which is why, amplitude of the successive paths is rapidly decreased and then it disappears.

Fig 17, & Fig 18. Show the multi-path propagation in Abu Dali district at a distance of 1000m and 5000m respectively. It is seen that the increase of the distance from sender to receiver and increase the number of paths led to grazing angle decreases, which is why, coefficient of reflection is increased [23]. The amplitude of consecutive paths won't be quickly decreased. Differences in the time between different paths are as low as possible. Which indicates the fact that the successive pathways will be converged with the time [12]. Multipath propagation dominates when there is more separation between the sender and receiver [30].

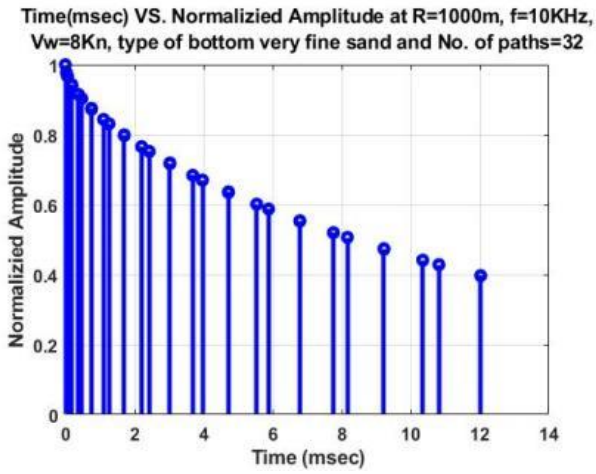

Figure 17. Multi-path propagation in Abu Dali district in Tigris River at, Zr=Zs=5m, D=12m, V_w=8Kn, R=1000m, S= 0.4944ppt, T=34ºC, f=10KHz and bottom type is very fine sands.

Table 2. the results of simulation have shown the T compared with φ, R_s, R_b and N.A

T	φ	R_s	R_b	N.A
0	0	1.0000	1.0000	1.0000
0.3283	13.4957	0.4685	0.5580	0.6939
0.6420	5.7106	0.8712	0.8096	0.5534
1.8693	18.778	0.2363	0.3438	0.2478
1.8693	7.9696	0.7652	0.7419	0.2478
3.7008	20.8068	0.1726	0.2895	0.0799
4.5926	13.4957	0.4685	0.5580	0.0487
7.1907	25.6410	0.0737	0.2156	0.0151

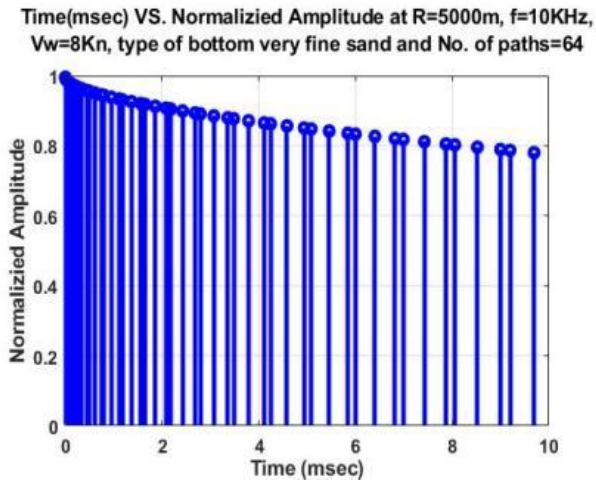

Figure 18. Multi-path propagations in Abu Dali district in Tigris River at, Zr=Zs=5m, D=12m, V_w=8Kn, R=5000m,

S= 0.4944ppt, T=34ºC, f=10KHz and bottom type is very fine sands.

7. Conclusions

This paper presented a detailed study of multipath propagation channel in Tigris River. The propagation of the sound is affected by the surface and the bottom reflections that become one of the main communication delays causes within system of underwater acoustic communications. Results have shown that acoustic path losses in the Tigris are increased with the increase of the communication range and frequency. By using Ray's model, results have shown that multi-path propagation is dominating in the case where distance from sender to receiver, has been increased resulting in decrease of grazing angle, thereby, resulting in the increase of coefficient of reflection. Successive paths' amplitude won't be quickly decreased. Which is why, differences in the time between various paths is as low as possible. Which is an indication of the fact that the successive path-ways will be converged with the time result in inter symbol interference phenomenon, playing a role in incrementing received data bit error rate. Thus, in general, UWACS supports the low levels of the data.

Acknowledgements

The authors want to thank soil lab, Dept. of Civil Engineering, and Environmental Labs, Dept. of Environmental Engineering, Engineering Faculty, Mustansiriyah University for supporting a research assistantship. This study is supported by the Department of Electricity, the Faculty of Engineering, Mustansiriyah University.

Conflicts of interest

There is no conflict that should be declared.

8. References

1. Chen, C., Zhu, H., Li, M., & You, S. (2018). A review of visual-inertial simultaneous localization and mapping from filtering-based and optimization-based perspectives. Robotics, 7(3), 45.
2. Li, S., Qu, W., Liu, C., Qiu, T., & Zhao, Z. (2019). Survey on high reliability wireless communication for underwater sensor networks. Journal of Network and Computer Applications, 148, 102446.
3. Ikpekha, O. (2017). Underwater acoustics propagation analysis and modelling of sound emitting devices (Doctoral dissertation, Dublin City University).
4. Burrowes, G., & Khan, J. Y. (2011). Short-range underwater acoustic communication networks. Autonomous Underwater Vehicles, 173-198.
5. Al-Aboosi, Y. Y., Ahmed, M. S., Shah, N. S. M., &Khamis, N. H. H. (2017). Study of absorption loss effects on acoustic wave propagation in shallow water using different empirical models. Journal of Engineering and Applied Sciences.
6. Melodia, T., Kulhandjian, H., Kuo, L. C., Demirors, E., Basagni, S., Conti, M., ... &Stojmenovic, I. (2013). Advances in Underwater Acoustic Networking.
7. Al-Aboosi, Y. Y., Bin Sha'ameri, A. Z., &Khamis, N. H. H. (2016). Comparison of methodologies for signal detection in underwater acoustic noise in shallow tropical waters. ARPN J EngApplSci, 11(5), 3086-3094.
8. Anandalatchoumy, S., &Sivaradje, G. (2015). Comprehensive study of acoustic channel models for underwater wireless communication networks. International Journal on Cybernetics & Informatics, 4(2), 227-240.
9. Borowski, B. (2009, October). Characterization of a very shallow water

acoustic communication channel. In OCEANS 2009 (pp. 1-10). IEEE.
10. Naidu, P. S. (2009). Sensor array signal processing. CRC press.
11. An, E. (2011). Underwater Channel Modeling for Sonar Applications (Doctoral dissertation, MSc Thesis, The Graduate School of Natural and Applied Sciences of Middle East Technical University).
12. Al_Aboosi, Y. Y., &Sha'ameri, A. Z. (2016). Experimental Multipath Delay Profile of Underwater Acoustic Communication Channel in Shallow Water. Indonesian Journal of Electrical Engineering and Computer Science, 2(2), 351-358.
13. Jensen, F. B., Kuperman, W. A., Porter, M. B., & Schmidt, H. (2011). Computational ocean acoustics. Springer Science & Business Media.
14. Khan, M. W., Zhou, Y., & Xu, G. (2014, November). Modeling of acoustic propagation channel in underwater wireless sensor networks. In The 2014 2nd International Conference on Systems and Informatics (ICSAI 2014) (pp. 586-590). IEEE.
15. Zanaj, E., Zanaj, B., Enesi, I., &Lumi, J. (2017, June). Link failure impact on the lifetime of WSN. In 2017 International Conference on Modern Power Systems (MPS) (pp. 1-4). IEEE.
16. Ahmad, W. (2016). Dynamic Packet Length Communication Technique for Underwater Sensor Networks.
17. Lanbo, L., Shengli, Z., & Jun-Hong, C. (2008). Prospects and problems of wireless communication for underwater sensor networks. Wireless Communications and Mobile Computing, 8(8), 977-994.
18. Babar, Z., Sun, Z., Ma, L., &Qiao, G. (2016, September). Shallow water acoustic channel modeling and OFDM simulations. In OCEANS 2016 MTS/IEEE Monterey (pp. 1-6). IEEE.
19. De Rango, F., Veltri, F., & Fazio, P. (2012, June). A multipath fading channel model for underwater shallow acoustic communications. In 2012 IEEE International Conference on Communications (ICC) (pp. 3811-3815). IEEE.
20. Yu, H., Yao, N., & Liu, J. (2015). An adaptive routing protocol in underwater sparse acoustic sensor networks. Ad Hoc Networks, 34, 121-143.
21. Zanaj, E., Gambi, E., Zanaj, B., Disha, D., & Kola, N. (2020). Underwater Wireless Sensor Networks: Estimation of Acoustic Channel in Shallow Water. Applied Sciences, 10(18), 6393.
22. Qiao, G., Babar, Z., Ma, L., Wan, L., Qing, X., Li, X., & Bilal, M. (2018, January). Shallow water acoustic channel modeling and MIMO-OFDM simulations. In 2018 15th International Bhurban Conference on Applied Sciences and Technology (IBCAST) (pp. 709-715). IEEE.
23. Kumar, P. P. (2019). UNDER WATER CHANNEL SIMULATION. PRATHEEK.
24. Sehgal, A., Tumar, I., &Schonwalder, J. (2009, May). Variability of available capacity due to the effects of depth and temperature in the underwater acoustic communication channel. In OCEANS 2009-EUROPE (pp. 1-6). IEEE.
25. Sehgal, A., Cernea, D., &Birk, A. (2010, May). Modeling underwater acoustic communications for multi-robot missions in a robotics simulator. In OCEANS'10 IEEE SYDNEY (pp. 1-6). IEEE.
26. Etter, P. C. (2013). Underwater Acoustic Modeling and Simulation. CRC Press.
27. De Rango, F., Veltri, F., & Fazio, P. (2012, June). A multipath fading channel model for underwater shallow acoustic

communications. In 2012 IEEE International Conference on Communications (ICC) (pp. 3811-3815). IEEE.
28. Etter, P. C. (2018). Underwater acoustic modeling and simulation. CRC press.
29. Fei, Y., Xiao-Yang, L., Qian, W., &En, C. (2014). Underwater Acoustic Communication Based on Hyperbolic Frequency Modulated M-ary Binary Orthogonal Keying. TELKOMNIKA Indonesian Journal of Electrical Engineering, 12(10), 7311-7317.
30. Prasanth, K. P. (2004). Modelling and simulation of an underwater acoustic communication channel. Master, Electronic Engineering University of applied sciences, Bremen, Germany.
31. Xiang-ping, G., &Rong-lin, H. (2011). Analyzing the performance of channel in Underwater Wireless Sensor Networks (UWSN). Procedia Engineering, 15, 95-99.
32. Bharti, P. (2016). A Study on Efficient Receiver Design for UWA Communication System (Doctoral dissertation, National Institute of Technology Rourkela).
33. Hodges, R. P. (2011). Underwater acoustics: Analysis, design and performance of sonar. John Wiley & Sons.
34. Khan, M. W., Zhou, Y., & Xu, G. (2014, November). Modeling of acoustic propagation channel in underwater wireless sensor networks. In The 2014 2nd International Conference on Systems and Informatics (ICSAI 2014) (pp. 586-590). IEEE.
35. Mohite-Patil, T. B., Saran, A. K., Sawant, S. R., &Mohite-Patil, T. T. (2010). Modeling of Acoustic Wave Absorption in Ocean. International Journal of Computer Applications, 9(12), 19-24.
36. Akyildiz, I. F., Pompili, D., &Melodia, T. (2006, September). State-of-the-art in protocol research for underwater acoustic sensor networks. In Proceedings of the 1st ACM international workshop on Underwater networks (pp. 7-16).
37. Stojanovic, M. (2008, January). Underwater acoustic communications: Design considerations on the physical layer. In 2008 Fifth Annual Conference on Wireless on Demand Network Systems and Services (pp. 1-10). IEEE.
38. Arnon, S., &Kedar, D. (2009). Non-line-of-sight underwater optical wireless communication network. JOSA A, 26(3), 530-539.
39. Li, B., Zhou, S., Stojanovic, M., Freitag, L., & Willett, P. (2008). Multicarrier communication over underwater acoustic channels with nonuniform Doppler shifts. IEEE Journal of Oceanic Engineering, 33(2), 198-209.
40. Gkoura, L. K., Roumelas, G. D., Nistazakis, H. E., Sandalidis, H. G., Vavoulas, A., Tsigopoulos, A. D., &Tombras, G. S. (2017). Underwater optical wireless communication systems: A concise review. In Turbulence Modelling Approaches—Current State, Development Prospects, Applications. InTech.
41. Akyildiz, I. F., Pompili, D., &Melodia, T. (2005). Underwater acoustic sensor networks: research challenges. Ad hoc networks, 3(3), 257-279.
42. Hubert, E., &Wolkersdorfer, C. (2015). Establishing a conversion factor between electrical conductivity and total dissolved solids in South African mine waters. Water Sa, 41(4), 490-500.
43. Panchal, S. S., &Pabari, J. P. (2019, March). Evaluation of Shallow Underwater Acoustical Communication Model for Attenuation and Propagation Loss for Aqueous Solution of Sodium Chloride. In 2019 International Conference on Recent

Advances in Energy-efficient Computing and Communication (ICRAECC) (pp. 1-5). IEEE.